

High-pressure single-crystal elasticity measurements of Al-Fe-bridgmanite support a Fe³⁺-rich pyrolitic lower mantle

A. Kurnosov¹, H. Marquardt¹, D.J. Frost¹, T. Boffa Ballaran¹, L. Ziberna^{1,2}

¹Bayerisches Geoinstitut BGI, University of Bayreuth, 95440 Bayreuth, Germany; ²now at University of Bristol, UK; *Correspondence to: Hauke.Marquardt@uni-bayreuth.de

The chemical composition of Earth's lower mantle can be constrained by combining seismological observations with mineral physics elasticity measurements¹⁻³. However, the lack of laboratory data for Earth's most abundant mineral (Mg,Fe,Al)(Al,Fe,Si)O₃ bridgmanite has hampered any conclusive result. Here, we report single-crystal elasticity data on Al-Fe-bearing bridgmanite (Mg_{0.9}Fe_{0.1}Si_{0.9}Al_{0.1})O₃ measured using high-pressure Brillouin spectroscopy and x-ray diffraction in a novel experimental approach. Our measurements show that the elastic behavior of Fe-Al-bearing bridgmanite is markedly different from the behavior of the MgSiO₃ endmember^{2,4}. We employ our data to model seismic wave velocities in the top portion of the lower mantle, assuming a pyrolitic⁵ mantle composition and accounting for depth-dependent changes in iron partitioning between bridgmanite and ferropericlasite^{6,7}. We find excellent agreement between our mineral physics predictions and the seismic Preliminary Reference Earth Model⁸ down to at least 1200 km depth, indicating chemical homogeneity of the upper and shallow lower mantle. A high Fe³⁺/Fe²⁺ ratio of about 2 in shallow lower mantle bridgmanite is required to match seismic data, implying the presence of metallic iron in an isochemical mantle. Our calculated velocities are in increasingly poor agreement with those of the lower mantle at depths >1200 km, indicating either a change in bridgmanite cation ordering or a decrease in the ferric iron content of the lower mantle.

Quantitative knowledge of the chemistry, mineralogy and temperature of the lower mantle is of key importance for interpreting the thermal evolution, geochemical properties, and dynamics of the Earth's interior. Pyrolite is a widely accepted model composition of the Earth's upper mantle⁵, which is broadly consistent with the composition of mantle rocks brought by volcanism to the Earth's surface. It remains unclear, however, if pyrolite is also representative of the composition of the lower mantle or if the 660 km seismic discontinuity that marks the transition to the lower mantle is also a chemical boundary². Direct constraints on the chemical and mineralogical composition of Earth's lower mantle can be derived through a comparison of seismic wave velocity models with synthetic mineral physics-based velocity models calculated from laboratory elasticity measurements^{1,2}. At conditions of the lower mantle, pyrolite composition rocks would be comprised of approximately 75 vol. % of (Mg,Fe,Al)(Fe,Al,Si)O₃ bridgmanite, 18 vol. % of (Mg,Fe)O ferropericlasite, and 7 vol. % of CaSiO₃ perovskite (Ca-Pv) (ref. 7).

Based on elasticity measurements on Al-bearing MgSiO₃, a recent study proposed that the lower mantle contains 93 vol.% of bridgmanite², thereby supporting the hypothesis of a chemical boundary between the upper and lower mantle. In the absence of experimental data on the elastic properties of Fe-Al-bearing bridgmanite, this interpretation was based on the elastic properties of Al-bearing but Fe-free bridgmanite. In the lower mantle, however, an energetically favorable coupled substitution of Fe³⁺ (ferric iron) and Al³⁺ for Mg²⁺ and Si⁴⁺ leads to an increased Fe³⁺-content in bridgmanite once Al³⁺ becomes available by the breakdown of majoritic garnet in the uppermost lower mantle⁹. The effect of coupled Fe³⁺/Al³⁺-substitution on the elastic properties and seismic wave velocities of bridgmanite, which has remained unconstrained by experiments, is therefore critical to construct reliable seismic models. In contrast to the experimentally derived

conclusion, computational studies that have attempted to predict the effects of Fe- and Al-incorporation on the bulk elastic properties of bridgmanite have proposed that a pyrolitic mantle may be consistent with seismic data^{10,11}. Here, we report simultaneous elastic wave velocity and density measurements on single-crystals of $(\text{Mg}_{0.9}\text{Fe}_{0.1}\text{Si}_{0.9}\text{Al}_{0.1})\text{O}_3$ bridgmanite, a composition very close to that expected for bridgmanite in a pyrolitic mantle⁷, to pressures of the lower mantle using a novel experimental approach (Fig. 1, see Methods). Single crystals of Al-Fe-bearing bridgmanite synthesized in a large volume multianvil press were parallel polished into disks and half-circle-shaped samples were cut using a focused ion beam¹². Two half-circular samples with different crystallographic orientations were loaded into the sample chamber of one diamond-anvil cell. Elasticity and density measurements were performed using a combined Brillouin scattering and x-ray diffraction system at the Bayerisches Geoinstitut.

A global fit of a third order Eulerian finite strain equation to all our high-pressure data yields the following best-fit elastic constants C_{ij} at room pressure, where the number in brackets refers to the 1σ -uncertainty in the last given digit: $C_{11} = 462.7$ (17) GPa; $C_{22} = 504.9$ (26) GPa; $C_{33} = 426.6$ (5) GPa; $C_{44} = 188.4$ (6) GPa; $C_{55} = 166.6$ (4) GPa; $C_{66} = 129.7$ (17) GPa; $C_{12} = 140.2$ (14) GPa; $C_{13} = 132.2$ (11) GPa; $C_{23} = 159.3$ (12) GPa. Figure 1c shows a comparison of the velocity dispersion in Al-Fe-bearing bridgmanite derived from this study to pure MgSiO_3 bridgmanite¹³ as well as computational results¹⁴. There is generally good agreement between our measured elastic constants for $(\text{Mg}_{0.9}\text{Fe}_{0.1}\text{Si}_{0.9}\text{Al}_{0.1})\text{O}_3$ and those predicted by computations for $(\text{Mg}_{0.9375}\text{Fe}_{0.0625}\text{Si}_{0.9375}\text{Al}_{0.0625})\text{O}_3$ (ref. 14) as shown in Extended Data Table 2.

From our global fit, we derive the following adiabatic bulk K_s and shear modulus G as well as their pressure-derivatives $K_{s,0}'$ and G_0' : $K_{s,0} = 250.8(4)$ GPa, $K_{s,0}' = 3.44(3)$, $G_0 = 159.7(2)$ GPa, $G_0' = 2.05(2)$. Comparison of our direct elasticity measurements to previous results on MgSiO_3

using Brillouin scattering^{13,15} and ultrasonics^{4,16,17} confirms that coupled Al/Fe-substitution
 lowers the bulk modulus as suggested based on high-pressure single-crystal XRD experiments¹⁸
 and computational work^{14,19}. Our data show that coupled Al/Fe-substitution also lowers the shear
 modulus, similarly to the effect observed for Al-incorporation alone^{2,20}. This experimental
 finding is consistent with computational results^{14,19} (Extended Data Figure 1). The fit to our data,
 however, requires a significantly larger pressure-derivative of the shear modulus as compared to
 pure MgSiO₃ ($G_0' = 1.6$) (refs. 4,21), Al-bearing bridgmanite containing 4-5 wt. Al₂O₃ ($G_0' =$
 1.6-1.7) (refs. 2,20), or bridgmanite containing mostly ferrous iron ($G_0' = 1.6$, Mg_{0.95}Fe_{0.05}SiO₃)
 (ref. 4). This observation points to a unique effect that coupled Al³⁺/Fe³⁺-substitution has on the
 shear elasticity of bridgmanite. We note that the pronounced increase of the derivative of the
 shear modulus is not captured by the previous computational studies that report only very minor
 changes of G_0' caused by the addition of the FeAlO₃ component to MgSiO₃ bridgmanite^{10,19}.
 From the derived elastic moduli and the measured densities, we calculated the average
 compressional and shear wave velocities of Fe-Al-bearing bridgmanite (Fig. 2). Our results show
 that Fe/Al-incorporation reduces the acoustic velocities at room pressure, but the stronger
 pressure dependence of the shear modulus leads to a shear velocity crossover with MgSiO₃
 bridgmanite at pressures of the lower mantle (Fig. 2).
 We use our elasticity results to model one-dimensional seismic wave velocity profiles for the
 uppermost lower mantle (Fig. 3, Extended Data Figure 2). For the models, we refine elastic
 properties for the bridgmanite (as well as ferropericlase) solid solution components based on our
 data and combine these with self-consistent thermodynamic determinations of the Fe-Mg
 partitioning between bridgmanite and ferropericlase to determine mineral compositions and
 seismic velocities with depth (see Methods). We did not include the upper ~100 km of the lower

mantle in our model as seismic wave speeds at these depths are influenced by the breakdown of majoritic garnet, which adds uncertainties to the modelling. Similarly, we did not extrapolate our model beyond a depth of 1350 km as the effects of the iron spin crossover in ferropericlasite and possibly in bridgmanite on the iron partitioning behavior as well as the elastic properties are not sufficiently quantified^{1,22}.

We calculated two possible seismic profiles based on different assumptions concerning the oxygen distribution in the mantle. This is motivated by previous experimental findings that show Al-bearing bridgmanite to always contain a large proportion of Fe^{3+} regardless of the redox conditions of the experiments^{23,24}, implying that the lower mantle contains significantly more ferric iron than the upper mantle. This observation allows for two possible scenarios²³, where (1) either the bulk oxygen content of the lower mantle is higher than that of the upper mantle, or (2) the bulk oxygen content remains constant throughout the mantle resulting in metallic iron formation in the lower mantle as a result of disproportionation of Fe^{2+}O to form metallic Fe and $\text{Fe}^{3+}_2\text{O}_3$ (ref. 23). In both models, we constrained the $\text{Fe}^{3+}/\Sigma\text{Fe}$ fraction in bridgmanite to a value of 0.66, consistent with the results of previous experiments carried out at shallow lower mantle conditions⁷. We find both our models to agree with the Preliminary Reference Earth Model (PREM)⁸ to a depth of 1200 km within 0.2%, i.e. within the range of expected uncertainties in seismic velocities in the lower mantle³. Our calculations therefore show that pyrolite is an excellent average model composition for the shallow lower mantle that can thus be considered isochemical to the upper mantle. This finding is consistent with geophysical observations that show slabs to enter the lower mantle²⁵, geodynamic simulations that favor whole mantle convection styles²⁶, as well as petrological findings of lower mantle inclusions in diamonds found on the Earth surface²⁷. Our low measured value of the pressure derivative of the bulk modulus

$K_{s,0}'$ confirms a previous prediction that $K_{s,0}'$ for bridgmanite would have to be below 4 in order for PREM velocities to be consistent with a pyrolitic mantle model²⁸.

The good agreement of our disproportionation model to PREM also indirectly supports a constant oxygen content in the mantle and the presence of a small amount of metallic iron as expected for a truly isochemical mantle²³. This finding is supported by the occurrence of iron metal inclusions in some sublithospheric diamonds²⁹. We note that the pressure range of our model is almost entirely covered by our experimental data on bridgmanite as well as available data for $(\text{Mg}_{0.9}\text{Fe}_{0.1})\text{O}$ ferropericlase³⁰ with almost the same chemical composition as expected in a pyrolitic mantle. Therefore, no significant extrapolations in pressure or composition are required (Extended Data Figures 3 and 4). The thermal parameters for the MgSiO_3 component are well constrained by recent experiments^{2,4} and computations³¹ and a recent computational study indicates only minor effects of the FeAlO_3 component on thermal elastic properties compared to MgSiO_3 (ref. 19). A model where all Fe and Al in bridgmanite is assumed to be accommodated by the FeSiO_3 and AlAlO_3 components provides a poor fit to PREM velocities (Fig. 3a).

Despite the excellent match of the absolute velocities found in our model to seismic data, our mineral physics models indicate a systematically increasing deviation of both compressional and shear wave velocities from PREM with depth (Figs. 3 & 4). This implies that the velocity gradients derived from seismology, which are tightly constrained by observations^{1,3}, are not fully captured by our model. It is important to note that our modelled shear and compressional velocities deviate from PREM in opposite directions. Therefore, the systematic difference between our model and PREM cannot be reconciled by employing a sub- or superadiabatic geotherm or by changing the major chemistry of the mantle with depth. Even though some uncertainties remain regarding the quantitative effects of the Fe^{2+} spin crossover in ferropericlase

on seismic wave velocities, it is likely that the change of spin state will further increase the systematic difference between our model and PREM as it causes a significant reduction in compressional wave velocities in ferropericlase with depth but only slightly affects shear wave velocities²². At greater depths the site ordering of Al and Fe in bridgmanite might change³². Such a process could impact on seismic velocities, but quantitative predictions are difficult. We find, however, that the velocity differences between our model and PREM can be minimized by allowing for a depth-dependent change of the ferric iron content in bridgmanite (Fig. 4). According to our calculations, a decrease of $\text{Fe}^{3+}/\Sigma\text{Fe}$ in bridgmanite from 0.66 at ~800 km depth to about 0.33 at a depth of ~1300 km results in velocity gradients of both shear and compressional velocities that match those of PREM within its uncertainties (Fig. 4). Such a possible decrease of ferric iron content in bridgmanite with depth would affect transport properties in the mantle, such as the electrical conductivity³³ and possibly mantle viscosity^{34,35}. Further work at higher pressures would be required, however, in order to test these predictions.

154 References

- 155 1 Cammarano, F., Marquardt, H., Speziale, S. & Tackley, P. J. Role of iron-spin transition in ferropericlasite on
 156 seismic interpretation: A broad thermochemical transition in the mid mantle? *Geophys. Res. Lett.* **37**,
 157 L03308 (2010).
- 158 2 Murakami, M., Ohishi, Y., Hirao, N. & Hirose, K. A perovskitic lower mantle inferred from high-pressure,
 159 high-temperature sound velocity data. *Nature* **485**, 90-94 (2012).
- 160 3 Cobden, L. *et al.* Thermochemical interpretation of 1-D seismic data for the lower mantle: The significance
 161 of nonadiabatic thermal gradients and compositional heterogeneity. *J. Geophys. Res.* **114**, B11309 (2009).
- 162 4 Chantel, J., Frost, D. J., McCammon, C. A., Jing, Z. & Wang, Y. Acoustic velocities of pure and iron-
 163 bearing magnesium silicate perovskite measured to 25 GPa and 1200 K. *Geophys. Res. Lett.* **39**, L19307
 164 (2012).
- 165 5 Ringwood, A. E. A model for the upper mantle. *J. Geophys. Res.* **67**, 857-867 (1962).
- 166 6 Nakajima, Y., Frost, D. J. & Rubie, D. C. Ferrous iron partitioning between magnesium silicate perovskite
 167 and ferropericlasite and the composition of perovskite in the Earth's lower mantle. *J. Geophys. Res.* **117**,
 168 B08201 (2012).
- 169 7 Irifune, T. *et al.* Iron Partitioning and Density Changes of Pyrolite in Earth's Lower Mantle. *Science* **327**,
 170 193-195 (2010).
- 171 8 Dziewonski, A. M. & Anderson, D. L. Preliminary reference Earth model. *Phys. Earth Planet. Inter.* **25**,
 172 297-356 (1981).
- 173 9 McCammon, C. Perovskite as a possible sink for ferric iron in the lower mantle. *Nature* **387**, 694-696
 174 (1997).
- 175 10 Wang, X., Tsuchiya, T. & Hase, A. Computational support for a pyrolitic lower mantle containing ferric
 176 iron. *Nature Geosci.* **8**, 556-559 (2015).
- 177 11 Zhang, S., Cottaar, S., Liu, T., Stackhouse, S. & Militzer, B. High-pressure, temperature elasticity of Fe-
 178 and Al-bearing MgSiO₃: Implications for the Earth's lower mantle. *Earth Planet. Sci. Lett.* **434**, 264-273
 179 (2016).
- 180 12 Marquardt, H. & Marquardt, K. Focused Ion Beam preparation and characterization of single-crystal
 181 samples for high-pressure experiments in the diamond-anvil cell. *Am. Mineral.* **97**, 299-304 (2012).
- 182 13 Sinogeikin, S. V., Zhang, J. & Bass, J. D. Elasticity of single crystal and polycrystalline MgSiO₃ perovskite
 183 by Brillouin spectroscopy. *Geophys. Res. Lett.* **31**, L06620 (2004).
- 184 14 Li, L. *et al.* Elasticity of (Mg, Fe)(Si, Al)O₃-perovskite at high pressure. *Earth Planet. Sci. Lett.* **240**, 529-
 185 536 (2005).
- 186 15 Yeganeh-Haeri, A. Synthesis and re-investigation of the elastic properties of single-crystal magnesium
 187 silicate perovskite. *Phys. Earth Planet. Inter.* **87**, 111-121 (1994).
- 188 16 Li, B. & Zhang, J. Pressure and temperature dependence of elastic wave velocity of MgSiO₃ perovskite and
 189 the composition of the lower mantle. *Phys. Earth Planet. Inter.* **151**, 143-154 (2005).
- 190 17 Sinelnikov, Y. D., Chen, G., Neuville, D. R., Vaughan, M. T. & Liebermann, R. C. Ultrasonic Shear Wave
 191 Velocities of MgSiO₃ Perovskite at 8 GPa and 800 K and Lower Mantle Composition. *Science* **281**, 677-
 192 679 (1998).
- 193 18 Boffa Ballaran, T. *et al.* Effect of chemistry on the compressibility of silicate perovskite in the lower
 194 mantle. *Earth Planet. Sci. Lett.* **333-334**, 181-190 (2012).
- 195 19 Shukla, G., Cococcioni, M. & Wentzcovitch, R. M. Thermoelasticity of Fe³⁺- and Al-bearing bridgmanite:
 196 Effects of iron spin crossover. *Geophys. Res. Lett.* **43**, 5661-5670 (2016).
- 197 20 Jackson, J. M., Zhang, J., Shu, J., Sinogeikin, S. V. & Bass, J. D. High-pressure sound velocities and
 198 elasticity of aluminous MgSiO₃ perovskite to 45 GPa: Implications for lateral heterogeneity in Earth's lower
 199 mantle. *Geophys. Res. Lett.* **32**, L21305 (2005).
- 200 21 Murakami, M., Sinogeikin, S. V., Hellwig, H., Bass, J. D. & Li, J. Sound velocity of MgSiO₃ perovskite to
 201 Mbar pressure. *Earth Planet. Sci. Lett.* **256**, 47-54 (2007).
- 202 22 Lin, J.-F., Speziale, S., Mao, Z. & Marquardt, H. Effects of the electronic spin transitions of iron in lower-
 203 mantle minerals: implications to deep-mantle geophysics and geochemistry. *Rev. Geophys.* **51**, 244-275
 204 (2013).
- 205 23 Frost, D. J. *et al.* Experimental evidence for the existence of iron-rich metal in the Earth's lower mantle.
 206 *Nature* **428**, 409-412 (2004).

- 24 Sinmyo, R., Hirose, K., Muto, S., Ohishi, Y. & Yasuhara, A. The valence state and partitioning of iron in the Earth's lowermost mantle. *J. Geophys. Res.* **116**, B07205 (2011).
- 25 Fukao, Y. & Obayashi, M. Subducted slabs stagnant above, penetrating through, and trapped below the 660 km discontinuity. *J. Geophys. Res.* **118**, 2013JB010466 (2013).
- 26 Tackley, P. J. Mantle Convection and Plate Tectonics: Toward an Integrated Physical and Chemical Theory. *Science* **288**, 2002-2007 (2000).
- 27 Walter, M. J. *et al.* Deep Mantle Cycling of Oceanic Crust: Evidence from Diamonds and Their Mineral Inclusions. *Science* **334**, 54-57 (2011).
- 28 Jackson, I. Elasticity, composition and temperature of the Earth's lower mantle: a reappraisal. *Geophys. J. Int.* **134**, 291-311 (1998).
- 29 Kaminsky, F. V. & Wirth, R. Iron Carbide Inclusions in Lower-Mantle Diamond from Juina, Brazil. *Can. Min.* **49**, 555-572 (2011).
- 30 Marquardt, H., Speziale, S., Reichmann, H. J., Frost, D. J. & Schilling, F. R. Single-crystal elasticity of (Mg_{0.9}Fe_{0.1})O to 81 GPa. *Earth Planet. Sci. Lett.* **287**, 345-352 (2009).
- 31 Zhang, Z., Stixrude, L. & Brodholt, J. Elastic properties of MgSiO₃-perovskite under lower mantle conditions and the composition of the deep Earth. *Earth Planet. Sci. Lett.* **379**, 1-12 (2013).
- 32 Catalli, K. *et al.* Effects of the Fe³⁺ spin transition on the properties of aluminous perovskite-New insights for lower-mantle seismic heterogeneities. *Earth Planet. Sci. Lett.* **310**, 293-302 (2011).
- 33 Xu, Y. & McCammon, C. Evidence for ionic conductivity in lower mantle (Mg,Fe)(Si,Al)O₃ perovskite. *J. Geophys. Res.* **107**, ECV 11-11-ECV 11-17 (2002).
- 34 Rudolph, M. L., Lekić, V. & Lithgow-Bertelloni, C. Viscosity jump in Earth's mid-mantle. *Science* **350**, 1349-1352 (2015).
- 35 Marquardt, H. & Miyagi, L. Slab stagnation in the shallow lower mantle linked to an increase in mantle viscosity. *Nature Geoscience* **8**, 311-314 (2015).

Acknowledgements: This research was supported through the projects “GeoMaX” funded under the Emmy-Noether Program of the German Science Foundation (MA4534/3-1) and the ERC advanced Grant no. 227893 “DEEP” funded through the EU 7th Framework Programme. The FEI Scios FIB machine at BGI Bayreuth is supported through grant INST 91/315-1 FUGG. We thank Johannes Buchen for assistance in creating figure 1c, Hubert Schulze for sample polishing and Katharina Marquardt for help with the FIB device.

AK, HM, DF, TBB designed the research. LZ synthesized the bridgmanite sample. AK performed the experiments and analysed the Brillouin data. TBB performed the XRD analysis. DF and HM discussed the content of the paper and performed the modelling. HM wrote the initial draft of the paper. All authors commented on the manuscript.

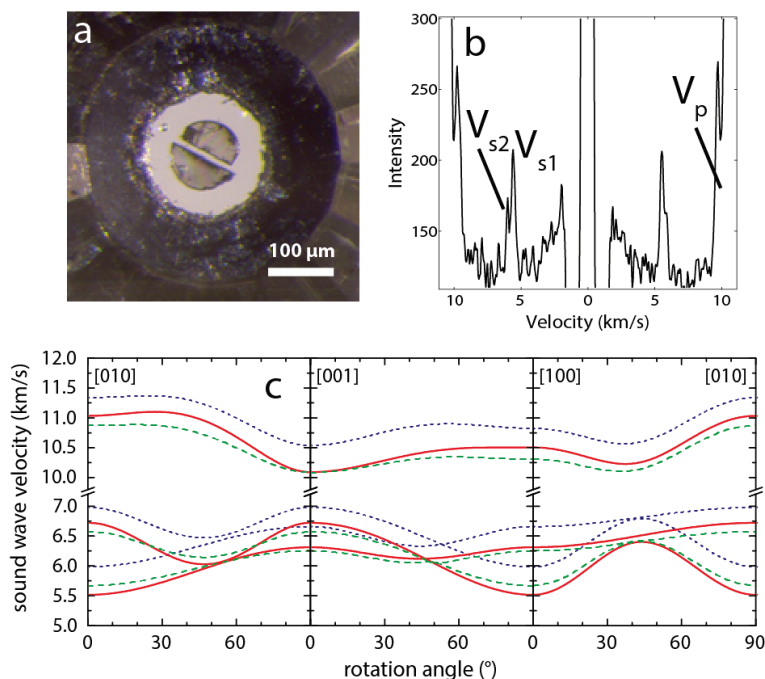
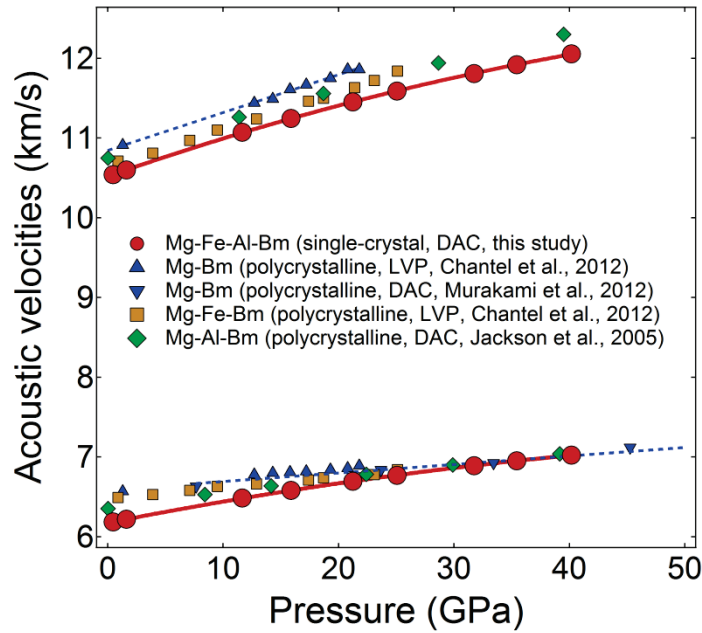


Figure 1. Experimental setup and results. (a) Two half-circular samples of single-crystal Al-Fe-bearing bridgmanite with different crystallographic orientations were loaded into the sample chamber of one diamond-anvil cell using helium as a pressure-transmitting medium. Elasticity and density measurements were performed using a combined Brillouin scattering and x-ray diffraction system at the Bayerisches Geoinstitut. A Brillouin spectrum collected at 31.8 GPa is shown in (b). Brillouin measurements were performed on both samples as a function of rotation angle. A least square fitting routine based on the Christoffel equation and finite strain equation was employed to solve for all nine independent non-zero elastic stiffness tensor components as a function of pressure (Extended Data Table 1). Primary pressure was calculated from the derived bulk modulus and measured unit cell volumes, eliminating the need to rely on a secondary pressure standard (see Methods). (c) Velocity dispersion curves at ambient conditions calculated from our work (red solid curves) in comparison to previous experimental work on MgSiO_3

255 bridgmanite¹³ (blue dotted curves) as well as computational work on Fe-Al-bearing bridgmanite¹⁴
 256 (green dashed curves).

257



258

259 **Figure 2.** Pressure-dependence of the average acoustic velocities of Al-Fe-bearing bridgmanite
 260 (red circles). The uncertainties in acoustic velocities are smaller than the symbol size. Previously
 261 published measurements on polycrystalline bridgmanite with different chemical compositions are
 262 shown for comparison (refs. 2,4,13,15,16,20,21). The blue dotted line indicates the pressure-trend
 263 of Mg-endmember bridgmanite: Fe/Al-incorporation reduces the acoustic velocities at room
 264 pressure, but the stronger pressure dependence of the shear velocities leads to a shear velocity
 265 crossover with MgSiO₃ bridgmanite at pressures above approximately 35 GPa.

266

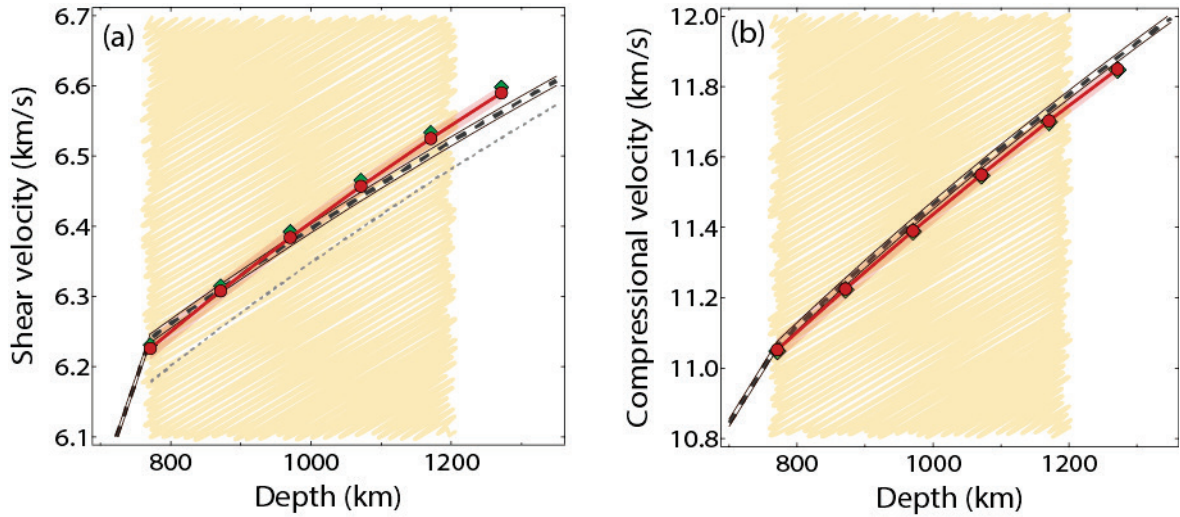


Figure 3. Comparison of mineral-physics based models of seismic shear (a) and compressional (b) velocities in the shallow lower mantle to PREM. Full symbols: Models that have been calculated assuming Fe^{2+} disproportionation (red) and assuming no disproportionation (green). The thermodynamic model not only matches available elasticity data for bridgmanite and ferropericlase (Extended Data Figures 3 and 4) but also reproduces changes in Fe-Mg partitioning between these phases with depth in both Al-free and Al-bearing systems (Extended Data Figure 5). The shaded region illustrates the Voigt and Reuss bounds for the red model. The thick dashed line shows the seismic PREM along with a 0.2 % uncertainty shown as thin lines. The scribbled area indicates the depth region where our pyrolitic seismic model agrees with the PREM within the Voigt-Reuss-bounds. The grey dotted line shows the results of our model when neglecting the FeAlO_3 component of bridgmanite.

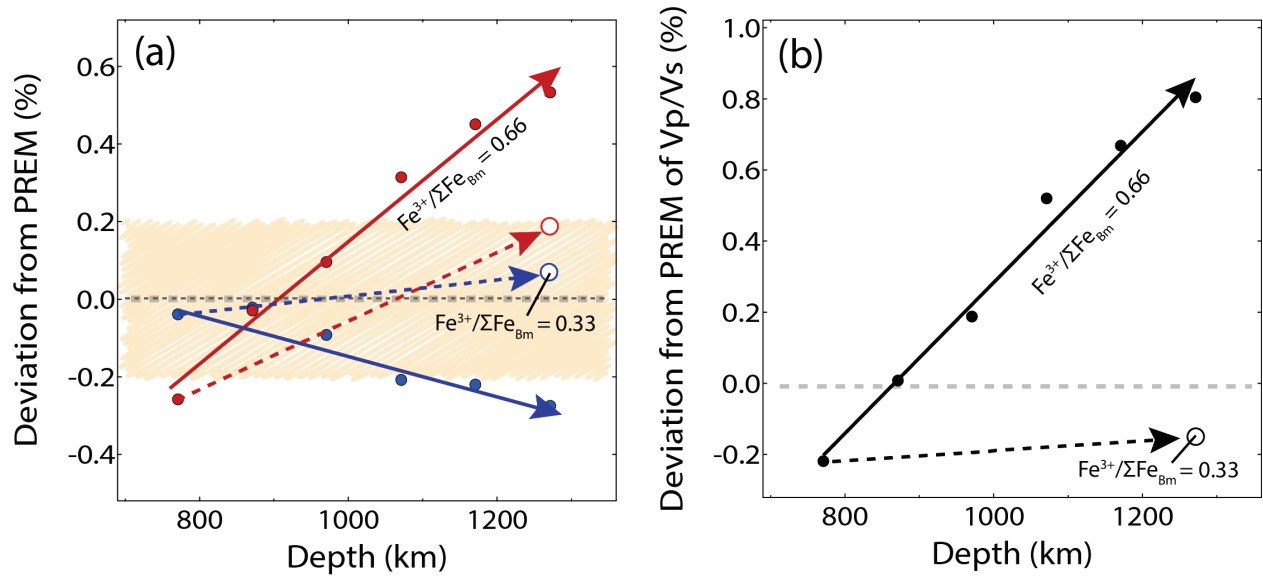


Figure 4. Deviation of modelled seismic velocities from PREM with depth. (a) Deviation of shear (red) and compressional velocities (blue) from PREM. The dashed region indicates 0.2 % uncertainty in seismic velocities. (b) Deviation of the V_p/V_s -ratio from PREM. The solid lines indicate the model results with the assumption of constant ferric iron content in bridgmanite. The dashed lines show results from the same model, but under the assumption that the ferric iron content in bridgmanite decreases with depth.